JOURNAL OF THERMOPHYSICS AND HEAT TRANSFER
Vol. 6, No. 3, July–Sept. 1992

Thermophoresis of a Radiating Aerosol in Laminar Boundary-Layer Flow

G. Jia,* J. W. Cipolla Jr.,† and Y. Yener‡
Northeastern University, Boston, Massachusetts 02115

The interaction between radiation and thermophoresis in forced convection laminar boundary-layer flow over an impermeable flat plate is investigated. The fluid is a radiatively nonparticipating constant-property gas containing emitting, absorbing, and isotropically scattering gray aerosol particles. The radiative properties of the gas–aerosol mixture are considered to be proportional to the local concentration of the particles in the mixture. The surface of the plate, maintained isothermal at a temperature lower than the freestream temperature, is assumed to be opaque, gray, and diffusely emitting and diffusely reflecting. Formal relations developed to the radiation part of the problem based on the Galerkin method are used together with the discretized forms of the energy and particle conservation equations to solve the problem numerically through an iterative scheme. The results show that radiation increases both the temperature gradients in the vicinity of the surface and the total heat flux to the surface, but decreases both the concentration of particles at the surface and the particle flux to the surface. It is also shown that with strong radiation the thermal boundary-layer thickness can increase up to one order of magnitude larger than the velocity boundary-layer thickness with an insignificant increase in the concentration boundary-layer thickness.

Nomenclature

Bo = Boltzmann number, Eq. (6)
C = aerosol particle concentration
c_p = specific heat of the background gas
D = Brownian diffusion coefficient
f = dimensionless stream function
I = total, directional radiation intensity
J_w = local particle flux to the cold plate
$\bar{J}_w$ = dimensionless local particle flux, Eq. (16)
K = thermophoretic coefficient
k = thermal conductivity of background gas
N_{CR} = conduction-to-radiation parameter, Eq. (7)
n = refractive index of the gas–aerosol mixture
Pr = Prandtl number
Q = dimensionless heat flux
q = heat flux in y direction
Re_x = local Reynolds number, $U_\infty x/\nu$
Sc = Schmidt number
T = temperature
U_∞ = freestream velocity
u = velocity in x direction
v = velocity in y direction
x = streamwise coordinate
y = normal coordinate
α = thermal diffusivity of the background gas
β = extinction coefficient
ε_w = surface emissivity
η = dimensionless, normal boundary-layer coordinate, Eq. (4)
Θ = dimensionless temperature, T/T_∞
κ = absorption coefficient
μ = direction cosine
ν = kinematic viscosity of the background gas
ξ = dimensionless, streamwise boundary-layer coordinate Eq. (5)
ρ = density of the background gas
σ = scattering coefficient
$\bar{\sigma}$ = Stefan-Boltzmann constant
τ = normal optical variable
ϕ = dimensionless concentration, C/C_∞
Ψ = dimensionless radiation intensity, $I/(n^2\bar{\sigma}T_\infty^4/\pi)$
ω = scattering albedo, $\sigma_\infty/\beta_\infty$

Subscripts
nr = quantities evaluated in the absence of radiation
w = quantities evaluated at the surface
∞ = quantities evaluated in the freestream

Superscripts
r = radiative quantity
T = total quantity, radiative plus conductive

Introduction

THE motion of ultrafine aerosols (i.e., submicrometer sized particles) suspended in a background gas can be strongly influenced by temperature gradients through the phenomenon of thermophoresis. This noncontinuum effect is responsible for particle deposition on cold surfaces in a variety of applications, including the Modified Chemical Vapor Deposition (MCVD) process by which optical fiber preforms are fabricated[1] for the deposition of soot in lamp chimneys and, most importantly, on cooled gas turbine blades.[2] The deposition of radioactive aerosol particles inside a nuclear reactor containment vessel following an accident is also strongly modified by the temperature gradients and is of major current interest for nuclear reactor safety.

Thermophoresis arises whenever the diameter of the aerosol particles is comparable to the mean-free-path of the background gas and is caused by the differential momentum transfer to the particles following collisions with molecules that originate in regions of the gas that differ in temperature. As a consequence, the particles experience a net force in the direction of decreasing temperature which, when balanced by viscous or molecular drag, gives rise to a steady particle velocity. This coupling between temperature gradients in the background gas and the spatial distribution of the aerosol particles is particularly interesting when the particles are at sufficiently high temperatures to participate in radiative trans-

Received March 27, 1991; revision received July 31, 1991; accepted for publication Aug. 1, 1991.

*Mechanical Engineering Department; currently, Senior Engineer, Thermoflow Inc., 888 Worcester Street, Wellesley, MA 02181.
†Professor and Chairman of Mechanical Engineering Department.
‡Professor of Mechanical Engineering.

fer and, therefore, are partially responsible for the temperature gradients in the background gas. In this case, the temperature field helps to determine the distribution of aerosol particles through thermophoresis. Since the radiative properties are dependent on the concentration of the aerosol and since the radiation field determines, in part, the temperature field, it is clear that radiating and thermophoretically moving aerosols are governed by a complicated nonlinear coupled set of energy and particle conservation equations. Although there has been very little research to date on the general problem of radiation coupled with aerosol motion through thermophoresis, it has already been demonstrated that thermophoresis can have a dramatic effect on the spatial distribution of aerosol particles and on the temperature in the medium.[3-5]

The problem of thermophoretic deposition of particles on a cold surface in flow systems of practical interest has attracted the attention of many researchers. Goren[6] gave a detailed theoretical analysis of compressible laminar flow with thermophoresis over a flat plate at zero incidence. He presented results for both hot and cold plates and discussed the thickness of the particle-free region found on heated objects. Epstein et al.[7] analyzed the thermophoretic deposition of small particles in natural convection flow over a cold vertical plate and gave results for both laminar and turbulent flow conditions. An external transverse flow situation past a circular cylinder has been studied by Homsy et al.,[8] Alam and Mehrotra,[9] and Garg and Jayaraj.[10] While Homsy et al.[8] used the Blasius series for solution, Alam and Mehrotra[9] used a numerical scheme. Garg and Jayaraj,[10] on the other hand, numerically integrated the governing nonlinear equations using automatic grid adaptation in the direction normal to the cylinder. Garg and Jayaraj[11] also presented a similar study over a plate inclined at an arbitrary angle. Shen[12] has studied the thermophoretic deposition of particles in two-dimensional and axisymmetric compressible flow fields onto cold cylindrical and spherical surfaces and discussed to what extent the particle concentration and the deposition rate at the wall are influenced by the density variations in the flow field. Recently, Gökoğlu and Rosner[13-15] have published a series of papers on thermophoretically augmented mass transfer rates in laminar as well as in turbulent boundary layers over a cold wall.

A scrutiny of the existing literature reveals that the important effects of thermal radiation on thermophoretic deposition in external flows have not been investigated. The objective of the present work is to study the interaction between thermophoresis and radiation in the steady and two-dimensional laminar boundary layer over a cold flat plate. The aerosol particles are assumed to be absorbing, emitting, isotropically scattering and gray, with their absorption and scattering coefficients being proportional to the local concentration of particles. It is also assumed that the aerosol is monodisperse and in thermal equilibrium with the radiatively nonparticipating background gas. In the following sections, we first present the formulation of the problem with the assumption of constant thermophysical and transport properties. Next, we use the formal relations developed to the radiation part of the problem by Jia et al.[16] together with the discretized forms of the energy and particle conservation equations to solve the problem numerically through an iterative scheme. Finally, we discuss the effects of various parameters of the problem on the temperature and aerosol concentration distributions, as well as on the heat transfer and particle flux to the plate.

Formulation

Consider a steady two-dimensional laminar boundary-layer flow of a gas containing suspended aerosol particles over an impermeable cold flat plate with uniform freestream velocity U_∞, temperature T_∞, and aerosol particle concentration C_∞. The aerosol particles are assumed to be absorbing, emitting, isotropically scattering, and gray. The plate is considered to be opaque, gray, and both diffusely reflecting and diffusely emitting with uniform emissivity over its surface, and maintained isothermal at T_w. It is also assumed that the aerosol is monodisperse, dilute, nonreactive and in thermal equilibrium with the radiatively nonparticipating background gas. Moreover, the aerosol particles are small enough for inertial effects to be ignored. Particles may be assumed to be in thermal equilibrium with the background gas if the thermal response time of the particle is small compared to the characteristic time of the changing flow conditions. For 1.0 μm SiO_2 particles the thermal response time is about 2.5 μs, so thermal equilibrium of such particles with a laminar boundary-layer flow seems reasonable. In addition small particles rapidly achieve hydrodynamic equilibrium. For example a 1-μm particle of unit density placed at rest in a flow of 10 m/s will achieve equilibrium with the flow after traveling 3.6×10^{-5} m.[17] These conclusions are also consistent with the work of Chomiak and Gupta.[18]

Assuming constant thermophysical properties for both the gas and the aerosol particles and neglecting viscous dissipation, the energy equation and the particle conservation equations, within the limitations of the boundary-layer approximations, may be written in dimensionless form as

$$\frac{1}{Pr}\frac{\partial^2\Theta}{\partial\eta^2} + \frac{f}{2}\frac{\partial\Theta}{\partial\eta} = \frac{df}{d\eta}\xi\frac{\partial\Theta}{\partial\xi} + \xi\phi\frac{\partial Q^r}{\partial\tau} \tag{1}$$

$$\frac{1}{Sc}\frac{\partial^2\phi}{\partial\eta^2} + \left(K\frac{1}{\Theta}\frac{\partial\Theta}{\partial\eta} + \frac{f}{2}\right)\frac{\partial\phi}{\partial\eta} = \frac{df}{d\eta}\xi\frac{\partial\Theta}{\partial\xi} - K\frac{\partial}{\partial\eta}\left(\frac{1}{\Theta}\frac{\partial\Theta}{\partial\eta}\right)\phi \tag{2}$$

with the conditions

$$\text{At } \eta = 0: \quad \Theta = \Theta_w, \quad \phi = 0 \tag{3a, b}$$

$$\text{As } \eta \to \infty: \quad \Theta \to 1, \quad \phi \to 1 \tag{3c, d}$$

$$\text{At } \xi = 0: \quad \Theta = \Theta_{nr}(\eta), \quad \phi = \phi_{nr}(\eta) \tag{3e, f}$$

where η and ξ, the dimensionless coordinates, are defined, respectively, as

$$\eta = \frac{y}{x}Re_x^{1/2} \tag{4}$$

$$\xi = \frac{\beta_\infty x}{Bo} = \frac{(\beta_\infty x)^2}{PrRe_x N_{CR}} \tag{5}$$

and the dimensionless stream function $f(\eta)$ is the solution of the well-known Blasius problem.[19] Moreover, the Boltzmann number Bo is defined as

$$Bo = \frac{\rho c_p U_\infty}{4n^2\bar{\sigma}T_\infty^3} \tag{6}$$

and the conduction-to-radiation parameter N_{CR} is given by

$$N_{CR} = \frac{k\beta_\infty}{4n^2\bar{\sigma}T_\infty^3} \tag{7}$$

In Eq. (2), $Sc = \nu/D$ is the Schmidt number where D denotes the Brownian diffusion coefficient, and K is the so-called thermophoretic coefficient, a dimensionless quantity that depends on the gas-to-particle ratio of thermal conductivities and on the ratio of the mean-free-path to the particle radius (i.e., the Knudsen number). The precise form of K has not yet been determined by a self-consistent theory valid for all values of the Knudsen number and thermal conductivity ratio. The best current expression is given by extrapolating the slip-region calculation of Brock[20] into the free-molecular regime and adjusting certain coefficients in order to recover

the free molecular limit as derived by Waldmann.[21] This has been presented in detail and compared with experiment by Talbot et al.[22] who conclude that this fitting formula should be accurate to within 20%. In the present work, we assume that both K and D are constants, independent of temperature.

In the conditions Eqs. (3e, f), $\Theta_{nr}(\eta)$ and $\phi_{nr}(\eta)$ are the self-similar solutions for the dimensionless temperature and particle concentration distributions, respectively, in the same problem in the absence of radiation (i.e., as $\beta_\infty \to 0$).

In Eq. (1), the dimensionless radiative heat flux Q^r is defined as

$$Q^r(\xi, \tau) = \frac{q^r(\xi, \tau)}{4n^2\bar{\sigma}T_\infty^4} = \frac{1}{2}\int_{-1}^{1} \Psi(\xi, \tau, \mu)\mu \, d\mu \qquad (8)$$

where q^r represents the radiative heat flux in the y direction, and the quantity τ denotes the optical variable defined as

$$\tau = \sqrt{\xi N_{CR} Pr}\int_0^\eta \phi(\xi, \eta') \, d\eta' \qquad (9)$$

If the absorption coefficient $\kappa(\xi, \eta)$ and the scattering coefficient $\sigma(\xi, \eta)$ are both considered to be proportional to the aerosol concentration according to

$$\kappa(\xi, \eta) = \kappa_\infty \phi(\xi, \eta) \quad \text{and} \quad \sigma(\xi, \eta) = \sigma_\infty \phi(\xi, \eta) \qquad (10a, b)$$

then, with the assumption that the gas-aerosol mixture is locally plane-parallel, the dimensionless radiation intensity satisfies the equation of radiative transfer given in the form

$$\mu \frac{\partial \Psi}{\partial \tau} + \Psi(\xi, \tau, \mu) = (1 - \omega)\Theta^4(\xi, \tau) + \frac{\omega}{2}\int_{-1}^{1} \Psi(\xi, \tau, \mu') \, d\mu' \qquad (11)$$

with the boundary conditions

$$\Psi(\xi, 0, \mu) = \varepsilon_w \Theta_w^4 + 2(1 - \varepsilon_w)\int_0^1 \Psi(\xi, 0, -\mu')\mu' \, d\mu', \quad \mu > 0 \qquad (12a)$$

$$\lim_{\tau \to \infty} \Psi(x, \tau, \mu) = 1, \quad -1 \le \mu \le 1 \qquad (12b)$$

where, the streamwise variations of Ψ appear parametrically.

It can also be shown that the derivative of the radiative heat flux in Eq. (1) is given by

$$\frac{\partial Q^r}{\partial \tau} = (1 - \omega)\left\{\Theta^4(\xi, \tau) - \frac{1}{2}\int_{-1}^{1} \Psi(\xi, \tau, \mu) \, d\mu\right\} \qquad (13)$$

For aerosol particles of interest in air at normal temperature and pressure the Schmidt number is very large, of the order of magnitude of 10^3 to 10^5. For example, for spherical particles of diameter 0.01 to 1.0 μm in air, the Schmidt number ranges from 3×10^2 to 5×10^5. Accordingly, in Eq. (2) we may neglect the Brownian diffusion compared to convection and thermophoresis and rewrite the particle conservation equation as

$$\left(K\frac{1}{\Theta}\frac{\partial \Theta}{\partial \eta} + \frac{f}{2}\right)\frac{\partial \phi}{\partial \eta} = \frac{df}{d\eta}\xi\frac{\partial \phi}{\partial \xi} - K\frac{\partial}{\partial \eta}\left(\frac{1}{\Theta}\frac{\partial \Theta}{\partial \eta}\right)\phi \qquad (14)$$

In this limit the Brownian diffusion sublayer is exponentially thin on the thermal and viscous boundary-layer scales and does not alter the thermophoretic particle deposition rate, as has been demonstrated rigorously by Gökoğlu and Rosner[14] using the method of matched asymptotic expansions. In the absence of Brownian diffusion, Eq. (14) is of first order in η, thus requiring only one boundary condition for ϕ in the η direction, and the condition Eq. (3b) is no longer imposed. Then, the solution of the particle concentration equation (Eq. (2)) yields a nonzero particle concentration at the surface of a cold plate. Strictly speaking, the nonzero concentration exists at the outer edge of the Brownian sublayer which, in the outer limit $\eta = 0(1)$, $Sc \to \infty$, is considered to be of negligible thickness.

The total local heat flux q_w^T to the plate will be composed of the heat fluxes due to heat conduction and radiation, and it can be calculated, in dimensionless form, as

$$Q_w^T = \frac{q_w^T}{4n^2\bar{\sigma}T_\infty^2} = \sqrt{\frac{N_{CR}}{\xi Pr}}\left(\frac{\partial \Theta}{\partial \eta}\right)_{\eta=0} - Q_w^r(\xi) \qquad (15)$$

where the first term on the right side represents the dimensionless heat flux to the plate due to conduction and the second term is the dimensionless radiative heat flux at the surface of the plate; that is, $Q_w^r(\xi) = Q^r(\xi, 0)$.

The local flux of particles J_w to the (cold) plate will be given by the thermophoretic flux and can be calculated, in dimensionless form, as

$$\bar{J}_w = (J_w/C_\infty U_\infty Re_x^{-1/2}) = K\left(\frac{\phi}{\Theta}\frac{\partial \Theta}{\partial \eta}\right)_{\eta=0} \qquad (16)$$

In this section we have presented the formulation of the problem. In the following sections we discuss the solution of the problem given here and present various results demonstrating the effects of the parameters of the problem on the temperature and particle concentration distributions as well as on the heat transfer to and particle deposition on the surface of the plate.

Solution

Having established the formulation of the problem, the solution of the interaction problem is now reduced to that of iterative calculations between the formal relations for Q^r and $\partial Q^r/\partial \tau$ developed in Ref. 16 and a numerical solution of the energy and particle conservation equations.

The procedure employed can be outlined as follows: The classical Blasius problem[17] is first solved by the use of a Runge-Kutta method and the dimensionless stream function $f(\eta)$ and its first derivative $df/d\eta$ are both obtained numerically. Next, the energy Eq. (1) and the particle conservation Eq. (14) are solved in the absence of radiation to obtain the no-radiation dimensionless temperature and concentration distributions: when radiation is absent, the energy and the particle conservation equations yield, for the conditions Eqs. (3a, c, d), self-similar solutions in the quadrature forms

$$\frac{\Theta_{nr}(\eta) - \Theta_w}{1 - \Theta_w} = \frac{\displaystyle\int_0^\eta \exp\left(-\frac{Pr}{2}\int_0^{\eta'} f(\eta'') \, d\eta''\right) d\eta'}{\displaystyle\int_0^\infty \exp\left(-\frac{Pr}{2}\int_0^{\eta'} f(\eta'') \, d\eta''\right) d\eta'} \qquad (17)$$

and

$$\phi_{nr}(\eta) = \exp\left\{-\int_\eta^\infty \frac{\dfrac{d}{d\eta'}\left(\dfrac{1}{\Theta_{nr}}\dfrac{d\Theta_{nr}}{d\eta'}\right)}{\dfrac{1}{\Theta_{nr}}\dfrac{d\Theta_{nr}}{d\eta'} + \dfrac{1}{2K}f(\eta')} d\eta'\right\} \qquad (18)$$

These solutions also represent the initial conditions for the dimensionless temperature and particle concentration distributions at $\xi = 0$ as indicated by Eqs. (3e, f). Once numerical

values first of $\Theta_{nr}(\eta)$ and then of $\phi_{nr}(\eta)$ are obtained from Eqs. (17) and (18), they are transformed into the forms $\Theta_{nr}(\xi_i, \tau)$ and $\phi_{nr}(\xi_i, \tau)$ at the next ξ_i by the use of the relation in Eq. (9). The temperature distribution $\Theta_{nr}(\xi_i, \tau)$ is now taken as a first approximation in the radiative transfer equation Eq. (11) and the relations developed in Ref. 16 based on the Galerkin method are employed to determine $Q^r(\xi_i, \tau)$. This approximate radiative heat flux is then transformed into the form $Q^r(\xi_i, \eta)$ again by the use of Eq. (9) and used in the simultaneous numerical solution of the energy equation Eq. (1) and the particle conservation equation Eq. (14) as described below to obtained new values for $\Theta(\xi_i, \eta)$ and $\phi(\xi_i, \eta)$. The procedure described above is then repeated until the differences between the last two calculated temperatures as well as the concentration distributions satisfy prescribed accuracies. Once the desired accuracies are reached, the dimensionless wall heat flux and the dimensionless particle flux to the cold plate are calculated from Eqs. (15) and (16), respectively. When calculations are completed at ξ_i, the above procedure is repeated at ξ_{i+1} where $\Theta(\xi_i, \eta)$ and $\phi(\xi_i, \eta)$ are used as the first approximations for the evaluation of $\Theta(\xi_{i+1}, \eta)$ and $\phi(\xi_{i+1}, \eta)$. A variable grid has been used in the discretization of η and ξ with a finer grid in the vicinity of the surface and at the leading edge of the plate. The number of subdivisions has been adjusted depending on conditions. For the results presented here, the total number of subdivisions in the normal direction was 200 to cover η from 0 to ∞, where ∞ was taken to be anywhere from 20 to 50 depending on the importance of the radiation and the extent of the radiation penetration depth. In the streamwise direction, the initial step size of ξ was taken to be as small as 0.001, for cases in which the radiation was strong, with the step size increasing farther from the leading edge. Numerical experiments were performed with as many as 1000 grid points normal to the plate to verify that the solutions were grid independent. Convergence was assumed to have occurred when the maximum relative difference in sequential iterates was less than 10^{-4} over all the grid points for both the temperature and concentration fields.

The energy equation Eq. (1), which is a parabolic equation with a source term, and the particle conservation equation Eq. (14) are both solved numerically in the above described calculations by the Crank-Nicholson scheme. In these calculations, the outer boundary is chosen large enough to include the whole thermal boundary layer, as well as the radiation penetration depth (see the section below on the results as well as the discussions in Ref. 16). Careful attention is specifically paid to the cases of strong radiation where the radiation penetration depth is significantly larger than the thermal boundary-layer thickness. In the following section, we present results to show the effects of various parameters of the problem on the temperature and particle concentration profiles, as well as on the heat and particle fluxes to the plate.

Results and Discussions

A selection of numerical results that illustrate the effects of the principal parameters of the problem on the temperature and aerosol concentration distributions is presented in this section. Although the dimensionless results hold for all cases we consider a specific model problem to give some indication of the magnitudes of the dimensional parameters. Thus we consider an aerosol of 0.1 μm SiO_2 spheres in air at 1000 K moving at 10 m/s with an initially uniform concentration of 2×10^{11} cm^{-1} over a black surface maintained at 500 K. Under these conditions scattering is negligible, and the Planck mean absorption coefficient has been calculated[23] to be $\kappa_\infty = 5$ m^{-1}. Using the thermophysical properties of air at the film temperature then gives $Bo = 22.25$, $N_{CR} = 0.001$, $K = 0.5$, and $\xi = 0.23x$ with x given in m. For these conditions the flow remains laminar for $0 \le x \le 4$ m so that the range of ξ becomes approximately $0 \le \xi \le 1$. These conditions are consistent with those occurring in the outside vapor deposition process for making optical fibers. In the following numerical calculation we have chosen a larger N_{CR} to show the interaction with conduction more clearly.

Figures 1 through 4 give the dimensionless temperature and aerosol concentration profiles as a function of η at several different values of the parameter ξ for $\varepsilon_w = 1$ (black boundary), $N_{CR} = 0.1$ (reasonably strong radiation), $\omega = 0$ (no scattering), $Pr = 0.7$ (gas), $K = 1$, and for two different values of Θ_w, that is, $\Theta_w = 0.2$ and 0.7. For a given value of the Boltzmann number Bo (i.e., convection-to-radiation parameter), the parameter ξ, defined by Eq. (5), represents the dimensionless quantity $\beta_\infty x$; therefore, ξ characterizes the di-

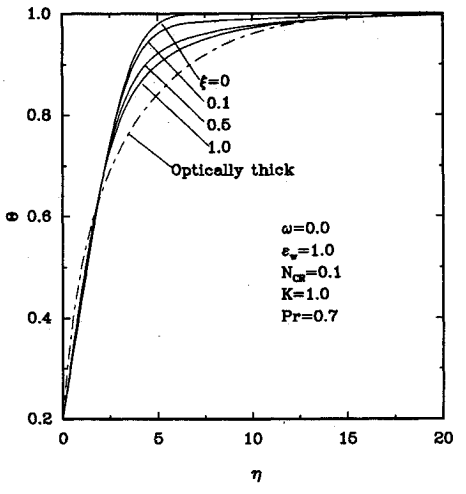

Fig. 1 The dimensionless temperature distribution with $\Theta_w = 0.2$.

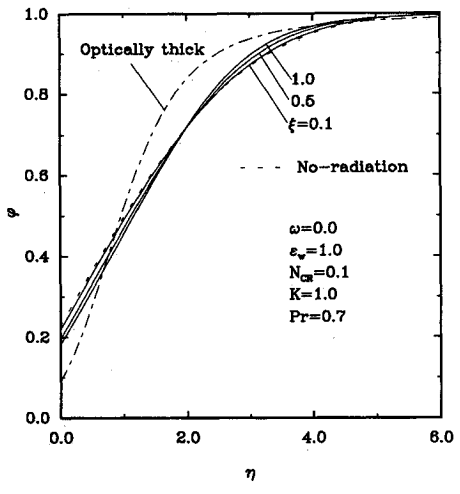

Fig. 2 The dimensionless concentration distribution with $\Theta_w = 0.2$.

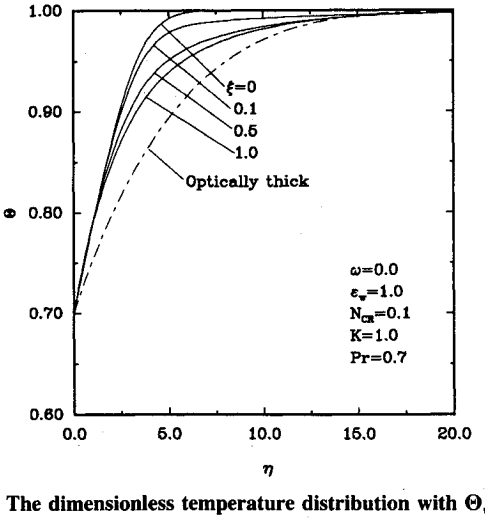

Fig. 3 The dimensionless temperature distribution with $\Theta_w = 0.7$.

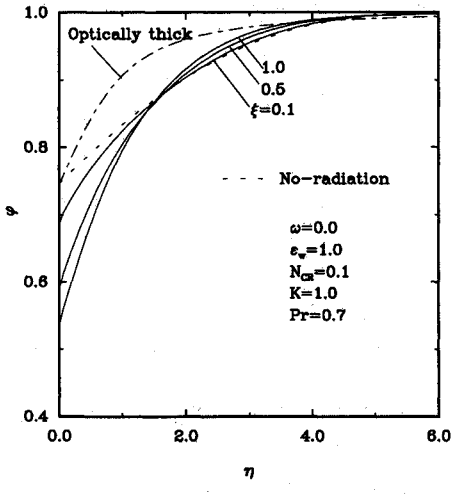

Fig. 4 The dimensionless concentration distribution with $\Theta_w = 0.7$.

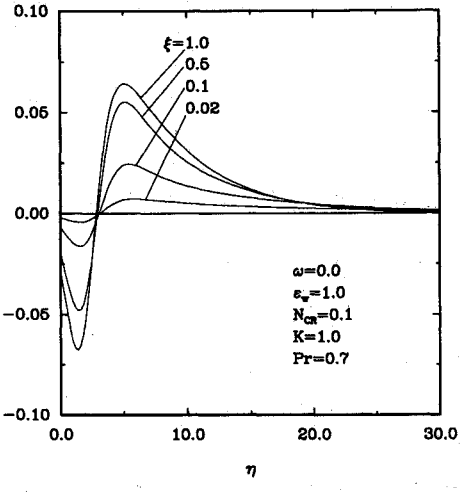

Fig. 5 The distribution of radiative dissipation with $\Theta_w = 0.2$.

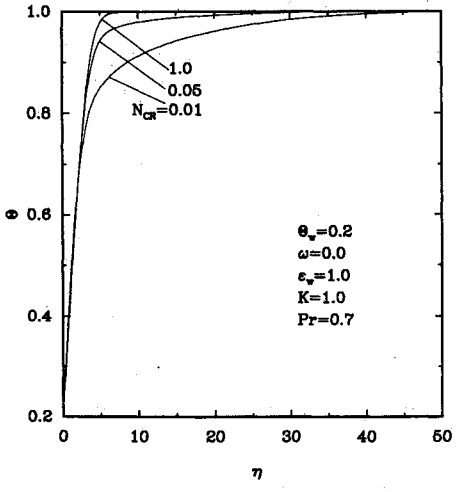

Fig. 6 The effect of N_{CR} on the temperature distribution with $\xi N_{CR} = 0.01$.

mensionless axial distance from the leading edge when β_∞ is specified, or it may be interpreted as demonstrating the effect of the extinction coefficient β_∞ (and therefore of radiation) at any x. On the other hand, ξ also demonstrates the effect of the Bo number (i.e., the effect of T_∞) for a given value of the product $\beta_\infty x$. Generally speaking, at any x, larger values of ξ correspond to stronger effects of radiation. In these figures, the temperature and concentration distributions for $\xi = 0$ correspond to the nonradiating case. Figures 1 through 4 also give the self-similar temperature and concentration profiles corresponding to the optically thick approximation (the Rosseland approximation). Figures 1 and 3 show that the effect of the parameter ξ is, in general, to increase the temperature gradients in the immediate vicinity of the (cold) plate (also see Table 1 and the results in Ref. 16) and to flatten the temperature profiles in the rest of the region, thereby significantly increasing the thickness of the thermal boundary layer. This behavior can be explained by referring to Fig. 5 which depicts the distribution of the radiative dissipation term $\xi\phi\partial Q^r/\partial\tau$ in the thermal boundary layer at various values of ξ for $\Theta_w = 0.2$. The radiative dissipation term, in fact, represents a source in the energy equation Eq. (1). The negative values of this quantity for small values of η indicate that the gas–aerosol mixture in the immediate vicinity of the (cold) plate absorbs more energy (from the hot external flow) than it emits. Subsequently, the temperatures near the plate and the temperature gradients at $\eta = 0$ increase and the temperature profiles away from the plate are flattened. Accordingly, the aerosol concentration in the vicinity of the plate decreases as ξ increases as depicted in Figs. 2 and 4. On the other hand, flattened but smaller temperatures away from the plate cause higher particle concentrations for larger values of η with increasing values of ξ.

In Fig. 4, the optically thick approximation gives an opposite trend for the case of $\Theta_w = 0.7$. The reason for this behavior is that the temperature gradients in regions close to the plate, which are the driving potentials for the formation of the concentration profiles, cannot be predicted correctly by the optically thick approximation when $\Theta_w = 0.7$.[16] Therefore, the optically thick approximation may not be a proper method to be used in this and similar studies.

Figures 6 and 7 show the temperature and concentration profiles as a function of η for various values of the conduction-to-radiation parameter N_{CR} with $\xi N_{CR} = 0.01$. The fixed value of the product ξN_{CR} implies that $\beta^2 x$ = constant for given values of the thermal diffusivity α and the free-stream velocity U_∞. Therefore, at any x, decreasing values of N_{CR} in these figures correspond to increasing values of T_∞ for a given value of the thermal conductivity k. On the other hand, since in these figures Θ_w = const., any increase in the value of T_∞ also indicates a corresponding increase in T_w. Thus, Figs. 6 and 7 illustrate, in fact, the effect on the temperature and concentration profiles of the simultaneous increases in T_∞ and T_w with decreasing values of N_{CR}.

Figures 8 and 9 give the boundary values of $(\partial\Theta/\partial\eta)_w$, the aerosol concentration ϕ_w and the dimensionless aerosol flux $\tilde{J}_w$ to the plate for $\Theta_w = 0.2$ and 0.7, respectively. The temperature gradient at $\eta = 0$ increases slightly with ξ, but the aerosol concentration at the wall ϕ_w decreases. On the other

Table 1 Effects of ε_w and ξ on $\tilde{J}_w$, ϕ_w, $(\partial\Theta/\partial\eta)_w$, Q_w^r, and Q_w^T

ε_w	ξ	$\tilde{J}_w$	ϕ_w	$(\partial\Theta/\partial\eta)_w$	$-Q_w^r$	$-Q_w^T$
1.0	0.00	0.27047	0.23013	0.23506		
	0.02	0.27046	0.22820	0.23703	0.21011	0.84360
	0.10	0.26760	0.22147	0.24137	0.17649	0.46543
	0.50	0.25693	0.20246	0.25382	0.12249	0.25816
	1.00	0.24909	0.19008	0.26652	0.09642	0.19548
0.5	0.02	0.27079	0.22675	0.23885	0.10792	0.74627
	0.10	0.26807	0.21511	0.24924	0.09248	0.39038
	0.50	0.25603	0.18361	0.27888	0.06735	0.21642
	1.00	0.24579	0.16499	0.29795	0.05504	0.16766
0.1	0.02	0.27105	0.22546	0.24044	0.02206	0.66467
	0.10	0.26838	0.20975	0.25591	0.01918	0.32505
	0.50	0.25511	0.16932	0.30133	0.01464	0.17571
	1.00	0.24289	0.14646	0.33168	0.01242	0.13778
0.0	0.02	0.27111	0.22515	0.24083	0.00000	0.64366
	0.10	0.26846	0.20839	0.25766	0.00000	0.30796
	0.50	0.25486	0.16584	0.30735	0.00000	0.16429
	1.00	0.24211	0.14201	0.34098	0.00000	0.12888

$\Theta_w = 0.2$, $\omega = 0.2$, $K = 1$, $N_{CR} = 0.1$ and $Pr = 0.7$.

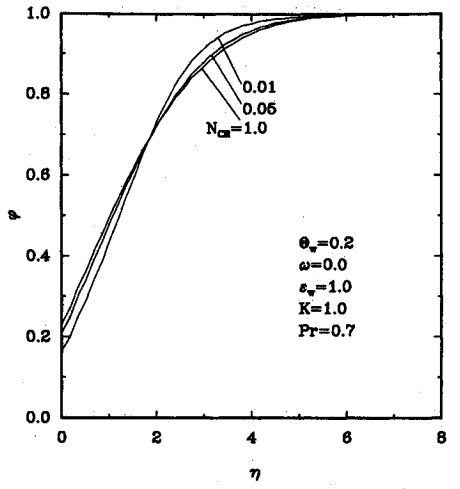

Fig. 7 The effect of N_{CR} on the concentration distribution with $\xi N_{CR} = 0.01$.

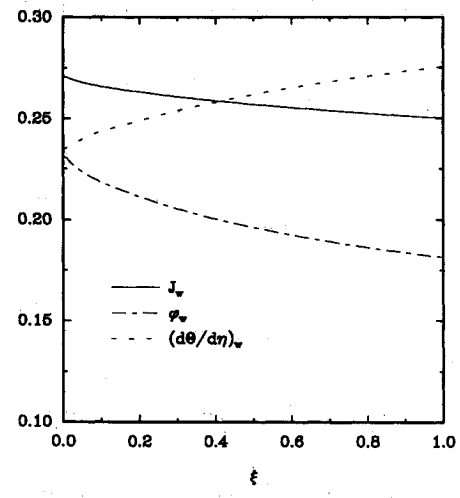

Fig. 8 The temperature gradient, aerosol flux, and particle concentration at the wall. ($\Theta_w = 0.2$, $\omega = 0$, $N_{CR} = 0.1$, $K = 1$ and $Pr = 0.7$)

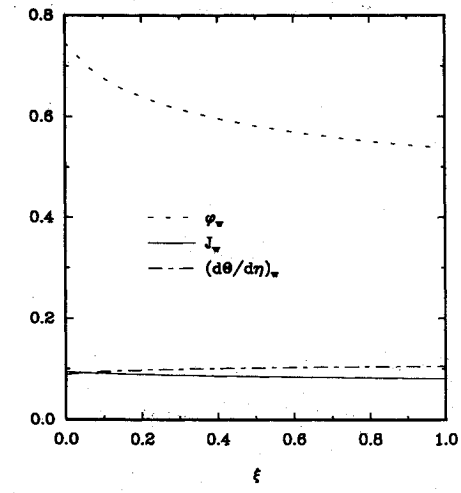

Fig. 9 The temperature gradient, aerosol flux, and particle concentration at the wall. ($\Theta_w = 0.7$, $\omega = 0$, $N_{CR} = 0.1$, $K = 1$ and $Pr = 0.7$)

hand, the aerosol flux $\bar{J}_w$, which is proportional to the product of the other two, decreases with ξ.

Figures 10 and 11 demonstrate the effect of the scattering albedo ω on the temperature and aerosol concentration profiles at $\xi = 1$. As expected, the effect of radiation becomes more pronounced for smaller values of ω. In these two figures, the profiles for $\omega = 1$ correspond to the nonradiating flow case.

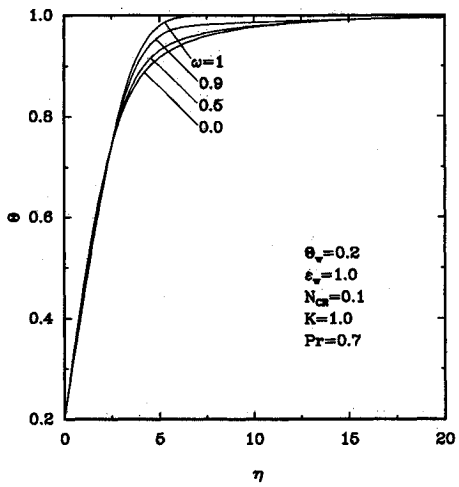

Fig. 10 The effect of ω on the temperature distribution at $\xi = 1.0$.

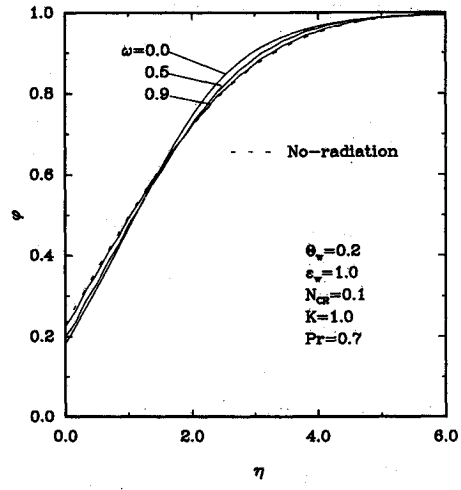

Fig. 11 The effect of ω on the concentration distribution at $\xi = 1.0$.

Table 2 Effects of K and ξ on $\bar{J}_w$ and ϕ_w

		$\Theta_w = 0.2$		$\Theta_w = 0.7$	
K	ξ	$\bar{J}_w$	ϕ_w	$\bar{J}_w$	ϕ_w
1.0	0.00	0.27047	0.23013	0.09388	0.74549
	0.02	0.27044	0.22755	0.09480	0.73329
	0.10	0.26693	0.21949	0.09305	0.69478
	0.50	0.25476	0.19695	0.08709	0.60399
	1.00	0.24566	0.18353	0.08084	0.55235
0.8	0.00	0.23538	0.25034	0.07769	0.77120
	0.02	0.23552	0.24749	0.07861	0.75940
	0.10	0.23291	0.23870	0.07754	0.72186
	0.50	0.22351	0.21432	0.07344	0.63234
	1.00	0.21611	0.19982	0.06858	0.58055
0.6	0.00	0.19555	0.27729	0.06054	0.80122
	0.02	0.19585	0.27409	0.06140	0.79005
	0.10	0.19419	0.26440	0.06094	0.75420
	0.50	0.18778	0.23775	0.05860	0.66740
	1.00	0.18228	0.22192	0.05518	0.61622
0.4	0.00	0.14890	0.31672	0.04220	0.83776
	0.02	0.14933	0.31307	0.04293	0.82765
	0.10	0.14886	0.30211	0.04297	0.79467
	0.50	0.14539	0.27258	0.04219	0.71372
	1.00	0.14199	0.25506	0.04019	0.66436
0.2	0.00	0.09093	0.38683	0.02232	0.88630
	0.02	0.09143	0.38234	0.02281	0.87812
	0.10	0.09163	0.36963	0.02311	0.85089
	0.50	0.09147	0.33635	0.02345	0.78324
	1.00	0.09028	0.31629	0.02277	0.73907

$\omega = 0$, $\varepsilon_w = 1$, $N_{CR} = 0.1$ and $Pr = 0.7$

Table 1 illustrates the effect of ε_w on the aerosol flux $\bar{J}_w$, the particle concentration ϕ_w, the temperature gradient $(\partial\Theta/\partial\eta)_w$ and on the dimensionless wall heat fluxes Q_w^r and Q_w^T. As seen from the results in Table 1, there is a strong coupling between the energy and particle conservation equations with increasing values of ε_w. The cases $\varepsilon_w = 1$ and $\varepsilon_w = 0$ correspond, respectively, to the black and totally reflecting boundaries at $\eta = 0$. As expected, with decreasing values of ε_w, the boundary fluxes $-Q_w^r$ and Q_w^T both decrease as the coupling between convection and radiation becomes weaker. On the other hand, with decreasing values of ε_w, $(\partial\Theta/\partial\eta)_w$ increases, resulting in lower values of ϕ_w and $\bar{J}_w$. This can be explained as follows: as depicted in Fig. 5, the fluid in the vicinity of the plate is absorbing more than it is emitting when $\Theta_w = 0.2$, thus yielding steeper temperature gradients in the presence of radiation. On the other hand, with decreasing ε_w (i.e., increasing surface reflectivity), the fraction of the absorbed energy that originates from higher temperature regions increases because of reflections from the plate and the fraction of the absorbed energy emitted from the cold boundary decreases due to smaller emissivity. Thus the net effect is that with a cold boundary, the temperature gradient increases and the particle concentration decreases in the vicinity of the plate as the emissivity decreases, with a net result of decreasing values of the particle flux to the plate.

Table 2 shows the effect of the thermophoretic coefficient K on the aerosol concentration at the boundary and the flux of aerosol particles to the plate as a function of ξ for two values of Θ_w, that is $\Theta_w = 0.2$ and 0.7. As seen, at any ξ, the flux $\bar{J}_w$ decreases and the concentration ϕ_w increases as the coupling between the temperature and particle concentration fields becomes weaker with decreasing values of K. As discussed earlier, for a given K, as ξ increases (i.e., as radiation gets stronger) the particle concentration in the vicinity of the plate and therefore ϕ_w decreases. On the other hand, as ξ increases, the flux $\bar{J}_w$ slightly increases initially before it starts decreasing. This behavior is a result of the product of decreasing ϕ_w and increasing $(\partial\Theta/\partial\eta)_w$ as ξ increases.

Acknowledgment

This work was partially supported by the National Science Foundation through Grant CBT-8603634.

References

[1]Simpkins, P. G., Greenberg-Kosinski, S., and MacChesney, J. B., "Thermophoresis: The Mass Transfer Mechanism in Modified Chemical Vapor Deposition," *Journal of Applied Physics*, Vol. 50, No. 9, 1979, pp. 5676–5681.

[2]Vermes, G., "Thermophoresis-Enhanced Deposition Rates in Combustion Turbine Blade Passages," *Journal of Engineering for Power*, Vol. 101, No. 4, 1979, pp. 542–548.

[3]Cipolla, J. W., Jr., and Morse, T. F., "Thermophoresis in an Absorbing Aerosol," *Journal of Aerosol Science*, Vol. 18, No. 3, 1987, pp. 245–260.

[4]Tse, T. S., Yener, Y., and Cipolla, J. W., Jr., "Aerosol Thermophoresis and Radiative Transfer," *Fundamentals and Applications of Radiation Heat Transfer*, A. M. Smith and T. F. Smith, eds., ASME/HTD-Vol. 72, 1987, pp. 59–65.

[5]Hannon, C., Yener, Y., and Cipolla, J. W., Jr., "Aerosol Thermophoresis with Conduction and Radiation," *Heat Transfer Phenomena in Radiation, Combustion, and Fires*, R. K. Shah, ed., ASME/HTD-Vol. 106, 1989, pp. 147–155.

[6]Goren, S. L., "Thermophoresis of Aerosol Particles in the Laminar Boundary on a Flat Plate," *Journal of Colloid and Interface Science*, Vol. 61, No. 1, 1977, pp. 77–85.

[7]Epstein, M., Hauser, G. M., and Henry, R. E., "Thermophoretic Deposition of Particles in Natural Convection Flow from a Vertical Plate," *Journal of Heat Transfer*, Vol. 107, No. 2, 1985, pp. 272–276.

[8]Homsy, G. M., Geyling, F. T., and Walker, K. L., "Blasius Series for Thermophoretic Deposition of Small Particles," *Journal of Colloid and Interface Science*, Vol. 83, No. 2, 1981, pp. 495–501.

[9]Alam, M. K., and Mehrotra, S., "Thermophoretic Deposition of Particles in Optical Fiber Preform Fabrication," ASME Paper, 87-HT-6, 1987.

[10]Garg, V. K., and Jayaraj, S. "Thermophoresis of Aerosol Particles in Laminar Flow over Inclined Plates," *International Journal of Heat Mass Transfer*, Vol. 31, No. 4, 1988, pp. 875–890.

[11]Garg, V. K., and Jayaraj, S., "Thermophoretic Transport of Aerosol Particles in Gas Flow over a Cylinder," AIAA 26th Aerospace Science Meeting, Paper AIAA-88-0656, Reno, NV, Jan. 1988.

[12]Shen, C., "Thermophoretic Deposition of Particles onto Cold Surfaces of Bodies in Two-Dimensional and Axisymmetric Flows," *Journal of Colloid and Interface Science*, Vol. 127, No. 1, 1989, pp. 104–115.

[13]Gökoğlu, S. A., and Rosner, D. E., "Viscous Dissipation Effects on Thermophoretically-Augmented Aerosol Particle Transport Across Laminar Boundary Layers," *International Journal of Heat Fluid Flow*, Vol. 6, No. 4, 1985, pp. 293–297.

[14]Gökoğlu, S. A., and Rosner, D. E., "Thermophoretically Augmented Mass Transfer Rates to Solid Walls Across Laminar Boundary Layers," *AIAA Journal*, Vol. 24, 1986, pp. 182–189.

[15]Gökoğlu, S. A., and Rosner, D. E., "Thermophoretically Enhanced Mass Transport Rates to Solid and Transpiration-Cooled Walls across Turbulent (Law-of-the-Wall) Boundary Layers," Industrial and Engineering Chemistry Fundamentals, Vol. 24, 1985, pp. 208–214.

[16]Jia, G., Yener, Y., and Cipolla, J. W., Jr., "Interaction of Radiation and Convection in Laminar Boundary Layer Flow over a Flat Plate," Presented at The 27th National Heat Transfer Conf., Minneapolis, MN, July 28–31, 1991.

[17]Hinds, W. C., *Aerosol Technology*, Wiley, New York, 1982.

[18]Chomiak, J., and Gupta, A. K., "Thermophoresis in Boundary Layer Flows," *Journal of Aerosol Science*, Vol. 20, No. 1, 1989, pp. 1–5.

[19]Kakac, S., and Yener, Y., *Convective Heat Transfer*, 2nd ed. (in print), Hemisphere, New York, 1991.

[20]Brock, J. R., "On the Theory of Thermal Forces Acting on Aerosol Particles," *Journal of Colloid and Interface Science*, Vol. 17, No. 8, 1962, pp. 768–780.

[21]Waldmann, L., *Zeitschrift fur Naturforschung*, Vol. A14, 1959, p. 590.

[22]Talbot, L., Cheng, R. K., Schefer, R. W., and Willis, D. R., "Thermophoresis of Particles in a Heated Boundary Layer," *Journal of Fluid Mechanics*, Vol. 101, Pt. 4, 1980, pp. 737–758.

[23]Paz, L. P., "The Effects of Thermal Radiation on the Laser Enhanced MCVD Process," Ph.D. Dissertation, Northeastern Univ., Boston, MA, 1990.